Liang Gong
School of Energy and Power Engineering,
Xi'an Jiaotong University,
Xi'an Shaanxi 710049, P.R. China
e-mail: lgong@mailst.xjtu.edu.cn

Krishna Kota
George W. Woodruff School of Mechanical Engineering,
Georgia Institute of Technology,
771 Ferst Drive NW,
Atlanta, GA 30332-0405
e-mail: krishna.kota@me.gatech.edu

Wenquan Tao
School of Energy and Power Engineering,
Xi'an Jiaotong University,
Xi'an Shaanxi 710049, P.R. China
e-mail: wqtao@mail.xjtu.edu.cn

Yogendra Joshi[1]
George W. Woodruff School of Mechanical Engineering,
Georgia Institute of Technology,
771 Ferst Drive NW,
Atlanta, GA 30332-0405
e-mail: yogendra.joshi@me.gatech.edu

Parametric Numerical Study of Flow and Heat Transfer in Microchannels With Wavy Walls

Wavy channels were investigated in this paper as a passive scheme to improve the heat transfer performance of laminar fluid flow as applied to microchannel heat sinks. Parametric study of three-dimensional laminar fluid flow and heat transfer characteristics in microsized wavy channels was performed by varying the wavy feature amplitude, wavelength, and aspect ratio for different Reynolds numbers between 50 and 150. Two different types of wavy channels were considered and their thermal performance for a constant heat flux of 47 W/cm^2 was compared. Based on the comparison with straight channels, it was found that wavy channels can provide improved overall thermal performance. In addition, it was observed that wavy channels with a configuration in which crests and troughs face each other alternately (serpentine channels) were found to show an edge in thermal performance over the configuration where crests and troughs directly face each other. The best configuration considered in this paper was found to provide an improvement of up to 55% in the overall performance compared to microchannels with straight walls and hence are attractive candidates for cooling of future high heat flux electronics. [DOI: 10.1115/1.4003284]

Keywords: wavy channels, heat transfer, thermal performance, electronics cooling, laminar fluid flow

1 Introduction

Thermal management is a key obstacle to scaling down the size of modern electronic devices. The power density of integrated circuits (ICs) is substantially higher than ever before according to the 2007 International Technology Roadmap for Semiconductors (ITRS) [1]. The maximum power of a single-chip high performance multiple purpose unit (MPU) will rise up to 47 W/cm^2 by the end of 2010, which will be very difficult to meet with the cooling efficiency of traditional fans. This increase in power density leads to significant thermal management problems, which if unaddressed, will severely limit miniaturization and functionality. One of the solutions proposed is to enhance heat transfer by utilizing single phase fluid flow in microchannels. Single phase flows are usually preferred owing to the low pressure drops. However, traditional microchannels still pose problems with high pressure drops because of the narrow flow passages or due to the presence of any additional/extraneous heat transfer enhancing the mechanisms.

Various passive enhancement techniques were suggested in literature to boost the performance of microchannel flows at high Re including the use of wavy surfaces for channel walls. Wavy channels are easy to manufacture and are a relatively cost-effective means to realize improved heat transfer performance passively. They were traditionally employed in high Re flows in large-scale heat exchangers [2] and recently in low Re and creeping flows in microfluidics and mixing applications as in lab-on-a-chip [3] and in microevaporators [4]. Kowalewski et al. [5] studied wavy channel ($\sim$1.6 mm hydraulic diameter) flows, with crests and troughs of the wavy structure facing each other, in the Re range of 1 to 3000, and observed the onset of flow instability at Re as low as 60. Hsieh and Huang [6] experimentally studied the role of different kinds of passive ribs in wavy microchannels (between 100 μm and 200 μm hydraulic diameters) in improving the mixing for $0.027 \leq Re \leq 0.081$.

Flow recirculation and mixing were observed with large wave amplitudes in pressure driven creeping flows above a critical Re. The value of critical Re depends on flow conditions and channel geometry. For creeping flows in microfluidic applications [3,6], the only mode of transport was found to be through diffusion. Hence, to promote mixing under such conditions (microchannel flows with $Re \ll 1$), artificial means were employed as in Refs. [7,8].

Observing that most of the prior investigations were concerned with large, or at least moderately large Reynolds number flows, or creeping flows, it appears interesting to study the transport phenomena for intermediate Reynolds number flows ($50 \leq Re \leq 150$), which can find many applications in cooling of electronics [9–14]. The considered Re range is also appropriate for liquid flows in microchannels (which provide substantially high heat transfer coefficients compared to air) for electronics cooling, (a) to avoid flow transition and (b) without employing any extraneous enhancement features that might complicate the implementation, both leading to large pressure drops. High pressure drops lead not only to an increase in pumping power but also pose a threat to the integrity (leakage of water into electronics) of the microchannels in the substrate and the IC assembly. Hence, the goal of this paper is to find out if there exists a possibility for improving the heat transfer using wavy microchannels without having a significant rise in the pressure drop (i.e., at $Re < 150$ which was not favored in prior attempts by researchers, e.g., in Ref. [9], in microchannel flows due to observed low heat transfer coefficients at those Re). Using numerical simulations, this was found to be possible by (i) promoting the periodic boundary layer thinning for improved heat transfer because of tailored wavy wall geometry and (ii) having a low Re which prevents flow transition and mixing that result in high pressure drops.

[1]Corresponding author.

Contributed by the Heat Transfer Division of ASME for publication in the JOURNAL OF HEAT TRANSFER. Manuscript received August 22, 2010; final manuscript received December 6, 2010; published online February 4, 2011. Assoc. Editor: Giulio Lorenzini.

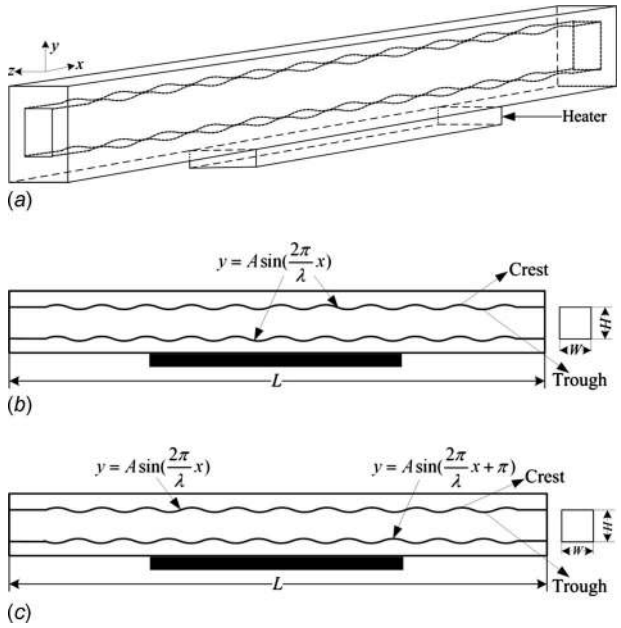

Fig. 1 Schematic of wavy channels

Two different types of wavy channels were traditionally employed: one with crests and troughs facing each other alternately by a phase of 180^0, i.e., $\Phi=\pi$ (serpentine channels, Fig. 1(*b*)) and the other with crests and troughs facing each other, i.e., $\Phi=0$ (raccoon channels, Fig. 1(*c*)). Therefore, both configurations were analyzed in this paper for different wave amplitude, wavelength, channel aspect ratio, and Re and a parametric study was performed to identify the geometry and flow conditions that contribute to an enhanced overall thermal performance. The schematic and the nomenclature of the channels are shown in Fig. 1.

The channel length was 20 mm with 2 mm straight sections at the inlet and the outlet. The wavy section spanned the middle 16 mm length of the channel with a hydraulic diameter of 500 μm. The parameters, wave amplitude A, wavelength λ, and the aspect ratio α, were varied independent of each other as functions of Re with a motivation to isolate and understand their individual impact on overall performance. Table 1 shows the values of the varied parameters in this study. The Reynolds numbers considered were 50, 100, and 150.

2 Numerical Simulation

The three-dimensional forced convection flow and heat transfer were modeled using a commercial computational fluids dynamics (CFD) solver, FLUENT [15], with the following assumptions and boundary conditions.

2.1 Assumptions

1. Steady, laminar flow
2. No thermophysical property variation with temperature
3. Fluid is incompressible, Newtonian, and viscous
4. No velocity-slip at the walls
5. Temperature and heat flux continuity at all the solid boundaries

Table 1 Range of variables considered for parametric study

A (in μm)=50,100,150,200	λ=2.0 mm, α=1.00
λ (in mm)=1.3,2.0,2.6,4.0	A=100 μm, α=1.00
α=1.00,1.25,1.67,2.50	A=100 μm, λ=2.0 mm

2.2 Governing Equations.

The steady-state conservation equations for mass, momentum, and energy in fluid are given by

$$\nabla\cdot(\rho\mathbf{u})=0 \tag{1}$$

$$(\mathbf{u}\cdot\nabla)\rho\mathbf{u}=-\nabla p+\mu\nabla^2\mathbf{u} \tag{2}$$

$$\mathbf{u}\cdot\nabla T=\frac{k}{\rho c_p}\nabla^2 T \tag{3}$$

Energy equation in the solid domain is given by

$$\nabla^2 T=0 \tag{4}$$

2.3 Boundary Conditions.

For the flow simulations, a uniform fluid inlet velocity was specified, along with the outlet pressure. For thermal simulations, a uniform fluid inlet temperature was specified and all the solid outer walls were assumed as insulated. A uniform heat source (constant wall heat flux condition) was assumed at the channel center in the flow direction on the other side (straight surface) of one of the two wavy surfaces, as shown in Fig. 1.

2.4 Grid Independency.

A hexahedral mapped mesh was used for all the simulations. Various grids of sizes from 10,000 nodes to 3.4 million nodes were employed for checking the mesh independency of the solution. The difference in the flow pressure drop and the Nusselt numbers between the solutions on the grids with 1.4 million and 3.4 million nodes was found to be about 0.4% and 0.3%, respectively. Hence, to save computing time and memory, grid sizes of around 1.4 million nodes were used for all the simulations in this study.

A relative error ε of less than 10^{-8} was assumed as the convergence criteria for velocity and pressure variables, while $\varepsilon<10^{-12}$ was assumed for temperature to stop the iterating procedure. The velocity-pressure coupling was achieved using the SIMPLEC [16] method.

3 Results and Discussion

Parametric heat transfer analysis was performed numerically for all the cases considered. A heat flux of 47 W/cm^2 [1] was assumed for a chip size of 1 cm^2 located at the channel center with respect to the flow direction (Fig. 1). An inlet temperature of 300 K was assumed. The wall material was assumed as copper and the fluid as water (Prandtl number=7).

To characterize the overall performance (by simultaneously considering the augmentation in both heat transfer and pressure drop), a performance factor was considered which compares the overall performance of a wavy channel with that of a straight channel based on the condition of a constant pumping power (as defined in Ref. [17]). Equation (5) shows the definition. The increase in surface area due to wall waviness was included in the calculations

$$PF=\frac{\left(\frac{\mathrm{Nu}_w}{\mathrm{Nu}_s}\right)}{\left(\frac{\Delta P_w}{\Delta P_s}\right)^{1/3}} \tag{5}$$

The PF was calculated for all the cases based on the numerical simulation results for pressure drop and wall averaged Nusselt number.

3.1 Effect of Wave Amplitude A

3.1.1 $\Phi=\pi$ *Configuration*. Figure 2 shows the Nu and Δp as a function of amplitude for $\Phi=\pi$ configuration. It can be observed that both Nu and Δp increase with A and Re. For the Re considered in the present study, the flow was found to be essentially streamlined and contoured along the walls of the wavy channels. The results showed no boundary layer separation even up to a Re

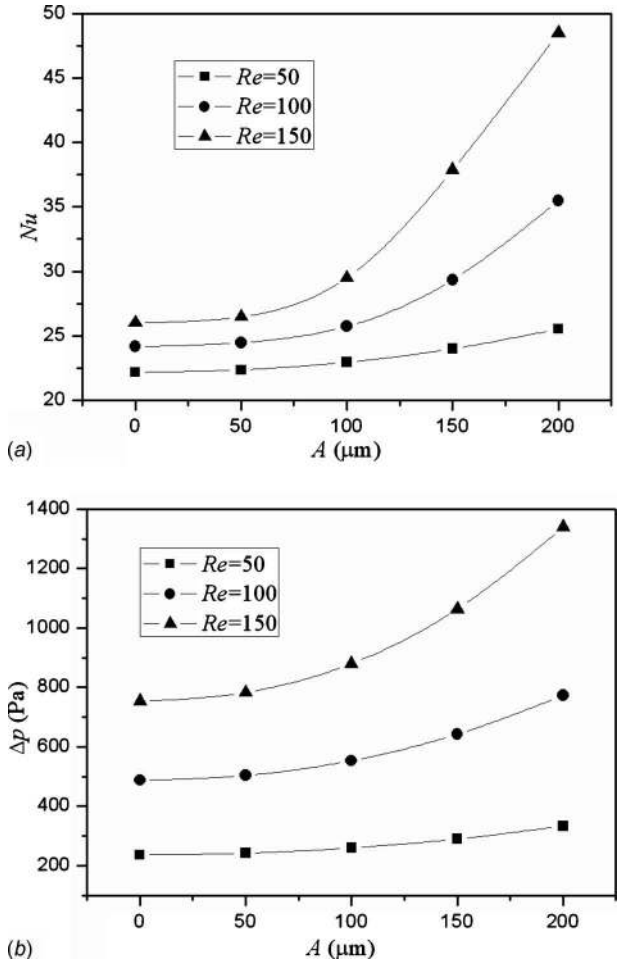

Fig. 2 Variation in (*a*) average Nusselt number and (*b*) pressure drop with amplitude

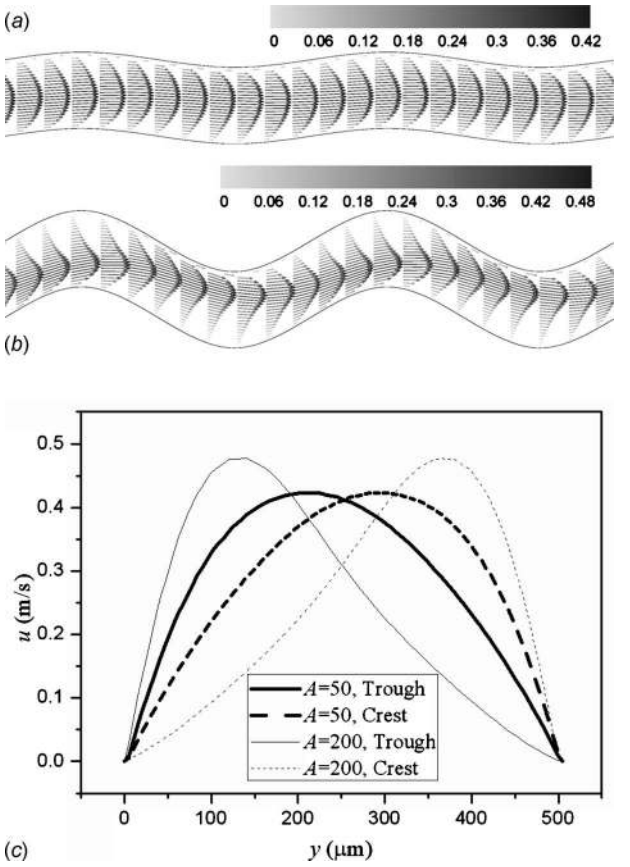

Fig. 3 (*a*) Velocity vectors for *A*=50 μm (top) and *A*=200 μm (bottom). (*b*) Spatial velocity contours for different wavelengths.

of 150, as seen in Fig. 3. Contrary to conventional observations of pressure driven flows in wavy channels, no vortical structure could be observed due to the low Re and microscale size of the channels. The flow seems to be dominated by viscous forces and a fully developed parabolic Poiseuille flow type behavior was exhibited, and no recirculations could be observed. Mathematically, no vortex generation can be attributed to a low Dean number (De), which is the product of Re and the curvature effect [18]. Critical De is ~956, after which Dean's vortices can be observed in such flows. Current cases with a low curvature and Re have a maximum De of <300 and so no vortex generation was observed.

As the amplitude is increased, it can be observed that the hydrodynamic boundary and thermal boundary layers are thinned due to the geometry governed biased shift of the maximum velocity from the centerline towards the wave peaks. This effect can be clearly observed in Fig. 3, wherein the velocity profile in the flow direction is plotted for $A=50$ μm and $A=200$ μm. This results in significantly enhanced thermal performance, which can be observed in Fig. 4, where the local Nusselt number as obtained from the simulation results can be found to be larger for $A=200$ μm near the wave peaks compared to $A=50$ μm at the same axial locations. The ratio of surface areas for the wavy and straight channels for all the cases in the paper (highest value being ~1.05) was far less than the Nusselt number ratio (highest being ~1.52), suggesting that increased surface area provides only a minor contribution to heat transfer improvement but it is the boundary layer thinning which is more important. The biased shift in the centerline velocity was also observed to occur with increasing Re. Due

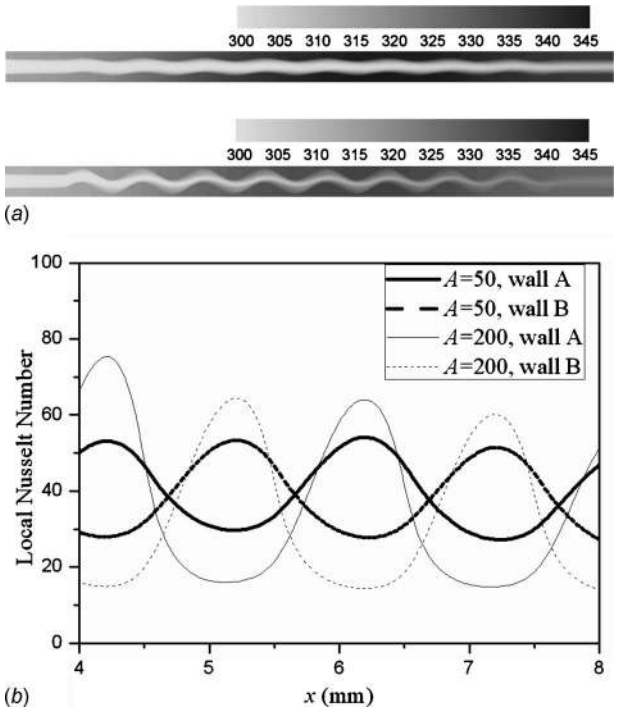

Fig. 4 (*a*) Temperature field for *A*=50 μm (top) and *A*=200 μm (bottom) and (*b*) local Nusselt number plot

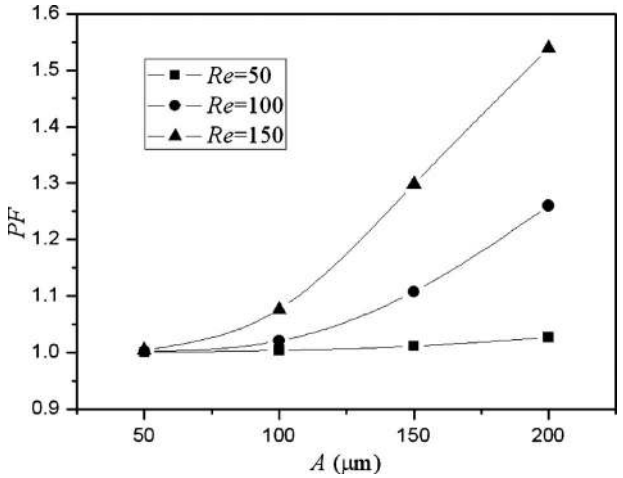

Fig. 5 Variation in *PF* with *A*

to the enhanced heat transfer for channels with high A, it was found that the maximum wall temperature also decreases as A and Re increase. The negative effect of increase in pressure drop for channels with higher amplitudes is overcome by the more dominant positive effect of increase in heat transfer, resulting in an improved overall performance, as shown in Fig. 5. Improved performance was also observed with increasing Re, also due to the reason discussed above.

3.1.2 $\Phi=0$ *Configuration*. Figure 6 shows the Nu and Δp as a function of amplitude for $\Phi=0$ configuration. It can be observed that both Nu and Δp increase with A and Re. Unlike the $\Phi=\pi$ configuration, $\Phi=0$ configuration showed boundary layer separation for high A, as could be seen in Fig. 7, and a vortex structure could be observed. The negative values of the flow directional velocity component confirm the existence of secondary flow for high A. This behavior was absent in channels with low A, wherein the geometry variation between expanding and contracting sections is not significant. For channels with high A, there exists a significant variation in the channel spanwise size since the hydraulic diameter is kept constant for all A (except for $\Phi=0$ configuration, where it is kept constant at the inlet and outlet) throughout this study.

Even though flow recirculation exists in channels with high A, the narrow contraction sections of the channels contribute to a significant increase in the pressure drop. The negative effect of increase in pressure drop for channels with higher amplitudes is overcome by the more dominant positive effect of increase in heat transfer at high Re, resulting in an improved overall performance, as shown in Fig. 8. This can be observed in Fig. 9 wherein the local Nusselt number was found to be larger for high A (150 μm) compared to an $A=50$ μm for Re=150. At low Re, *PF* was found to decrease with increasing A due to the high pressure drops associated with flow at the contraction sections of the channels, which dominated the improvement in heat transfer. For high Re, due to the enhanced heat transfer for channels with high A, it was found that the maximum wall temperature also decreases as A and Re increase.

3.2 Effect of Wavelength λ

3.2.1 $\Phi=\pi$ *Configuration*. Figure 10 shows the Nu and Δp as a function of wavelength for $\Phi=\pi$ configuration. It can be observed that both Nu and Δp decrease with λ (also, represented as *WL*) and increase with Re. The results showed no boundary layer separation even up to a Re of 150, as seen in Fig. 11. The flow was found to be essentially streamlined and contoured along the

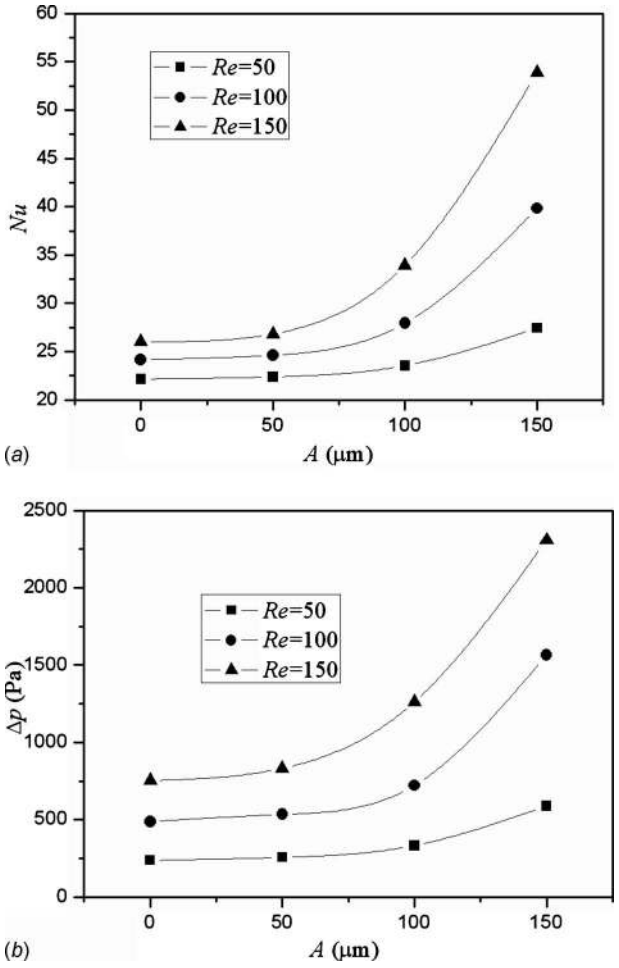

Fig. 6 Variation in (*a*) average Nusselt number and (*b*) pressure drop with amplitude

walls of the wavy channels as observed before.

As the wavelength is decreased, it can be observed that the hydrodynamic boundary and thermal boundary layers are thinned due to the geometry governed biased shift of the maximum velocity from the centerline towards the wave peaks. This effect can be clearly observed in Fig. 11, wherein the velocity profile in the flow direction is plotted for $\lambda=1.33$ mm and $\lambda=4$ mm. The effect of lowering the wavelength is analogous to increasing the amplitude (or compressing the wave between two fixed points spaced at a distance equal to the channel length). This results in significantly enhanced thermal performance, which can be observed in Fig. 12, where the local Nusselt number as obtained from the simulation results can be found to be larger for $\lambda=1.33$ mm near the wave peaks compared to $\lambda=4$ mm at the same axial locations. The biased shift in the centerline velocity was also observed to occur with increasing Re. Due to the enhanced heat transfer for channels with low λ, it was found that the maximum wall temperature also decreases as λ decreases and Re increases.

The negative effect of increase in pressure drop for channels with lower wavelengths is overcome by the more dominant positive effect of increase in heat transfer resulting in an improved overall performance, as shown in Fig. 13. Improved performance was also observed with increasing Re, also due to the reason discussed above. It is interesting to note that there exists an optimum wavelength (here, 2 mm) below which the adverse impact of pressure drop increase subsides the marginally improved heat transfer performance, resulting in a decrease in the overall perfor-

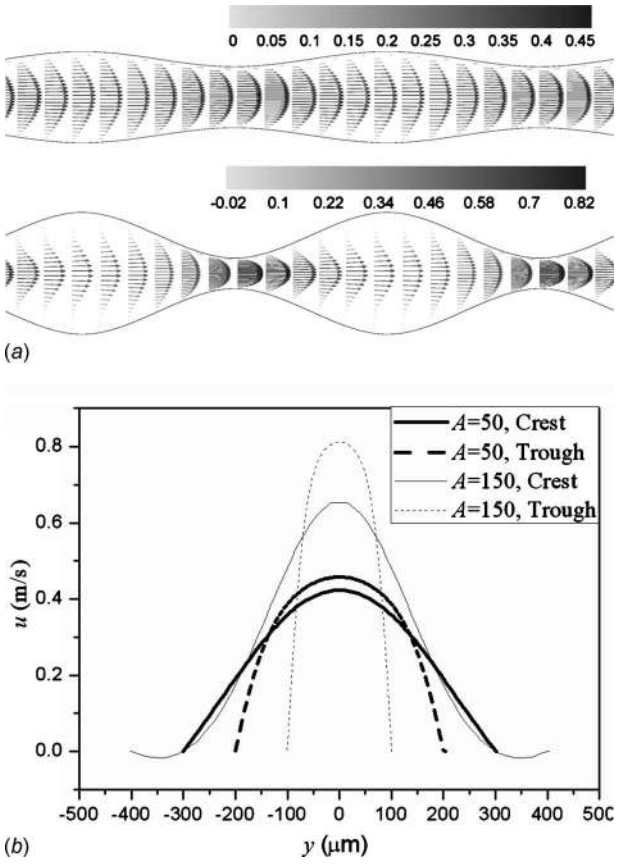

Fig. 7 (*a*) Velocity vectors for $A=50$ μm (top) and $A=150$ μm (bottom). (*b*) Spatial velocity contours for different wavelengths

mance. This can be clearly understood by observing the change in the slope of the performance curves, especially at high Re, in Fig. 13 for $\lambda=2$ mm.

3.2.2 $\Phi=0$ *Configuration*. Figure 14 shows the Nu and Δp as a function of wavelength for $\Phi=0$ configuration. It can be observed that both Nu and Δp increase with decreasing λ and increasing Re. Unlike the $\Phi=\pi$ configuration, $\Phi=0$ configuration showed boundary layer separation for low λ (reminiscent of high A), as could be seen in Fig. 15, and a vortex structure could be observed. The negative values of the flow directional velocity component in Fig. 15 confirm the existence of secondary flow for low λ. This behavior was absent in channels with high λ, wherein the geometry variation between expanding and contracting sections is not significant. For channels with low λ, there exists a significant variation in the channel spanwise area.

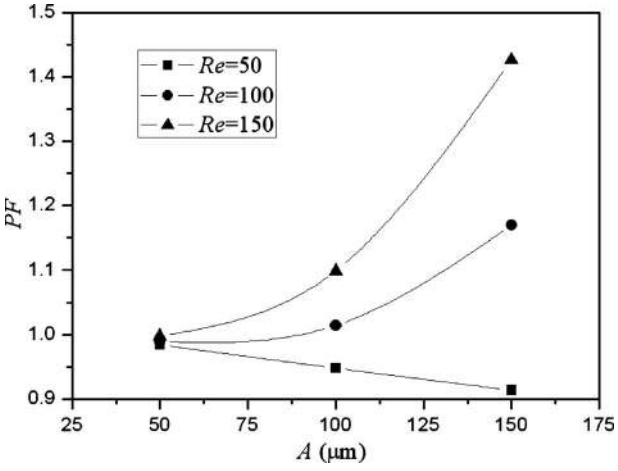

Fig. 8 Variation in *PF* with *A*

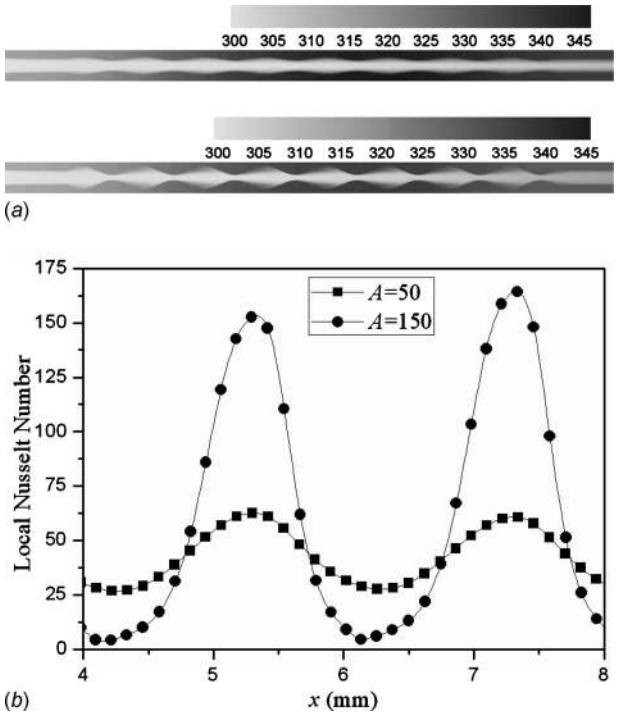

Fig. 9 (*a*) Temperature field for $A=50$ μm (top) and $A=150$ μm (bottom) and (*b*) local Nusselt number plot

Even though flow recirculation exists in channels with low λ, the narrow contraction sections of the channels contribute to a significant increase in the pressure drop. The negative effect of the increase in pressure drop for channels with lower wavelengths is overcome by the more dominant positive effect of the increase in heat transfer resulting in an improved overall performance, as shown in Fig. 16. This can be observed in Fig. 17 wherein the local Nusselt number is plotted as a function of the channel length. Enhancement can be observed for channel with low λ both in terms of the peak local value and the number of peaks. Improved performance was also observed with increasing Re, also due to the reason discussed above. Unlike with $\Phi=\pi$ configuration, no optimum was observed with $\Phi=0$ configuration because of continuously increasing and large pressure drops with decreasing λ (from Fig. 14). Due to the enhanced heat transfer for channels with low λ, it was found that the maximum wall temperature also decreases as λ decreases and Re increases.

3.3 Effect of Channel Aspect Ratio α

3.3.1 $\Phi=\pi$ *Configuration*. Figure 18 shows the Nu and Δp as a function of aspect ratio for $\Phi=\pi$ configuration. It can be observed that both Nu and Δp increase with α and Re. The results showed no boundary layer separation even up to a Re of 150, as seen in Fig. 19. The flow was found to be essentially streamlined and contoured along the walls of the wavy channels as observed before. As the aspect ratio is increased (keeping the same hydraulic diameter), it can be observed that the hydrodynamic boundary and thermal boundary layers are thinned due to the decreasing effect of W compared to H for higher aspect ratios. This effect can be clearly observed in Fig. 19, wherein the velocity profiles in the flow direction is plotted for $\alpha=1$ and $\alpha=2.5$. This results in an increase in the Nu. This results in enhanced thermal performance,

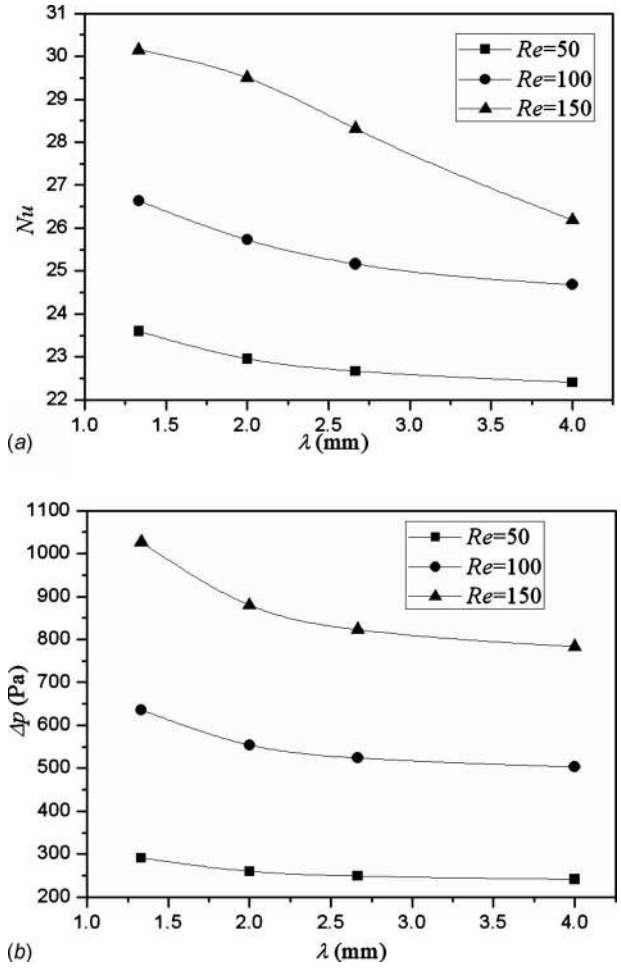

Fig. 10 Variation in (*a*) average Nusselt number and (*b*) pressure drop with wavelength

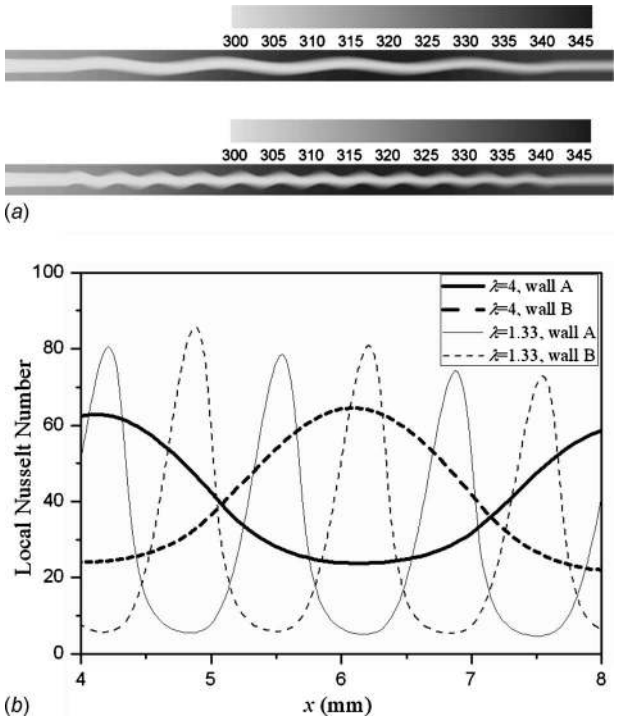

Fig. 12 (*a*) Temperature field for λ=4 (top) and λ=1.33 (bottom) and (*b*) local Nusselt number plot

which can be observed in Fig. 20, where the local Nusselt number on an average as obtained from the simulation results can be found to be larger for $\alpha=2.5$ compared to $\alpha=1$. Due to the enhanced heat transfer for channels with high α, it was found that the maximum wall temperature also decreases as α and Re both increase.

The pressure drop increases considerably with α when Re is kept the same as in the present study. The negative effect of the increase in pressure drop for channels with higher aspect ratios dominates the positive effect of the increase in heat transfer, resulting in an optimum performance condition, as shown in Fig. 21. Improved performance was also observed with increasing Re, also due to the boundary layer thinning, as discussed in prior subsections.

3.3.2 $\Phi=0$ *Configuration*. Figure 22 shows the Nu and Δp as a function of aspect ratio for $\Phi=0$ configuration. It can be observed that both Nu and Δp increase with increasing α and Re. As α is made larger, the contraction sections became much thinner, resulting in a significant increase in the pressure drops. The negative effect of the increase in pressure drop for channels with higher aspect ratios dominated the positive effect of the increase in heat transfer (due to thinner boundary layers), resulting in an optimum overall performance, as shown in Fig. 23. The local

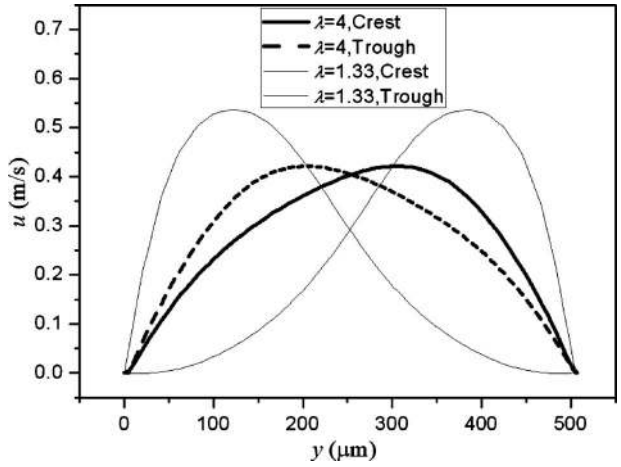

Fig. 11 Spatial velocity contours for different wavelengths

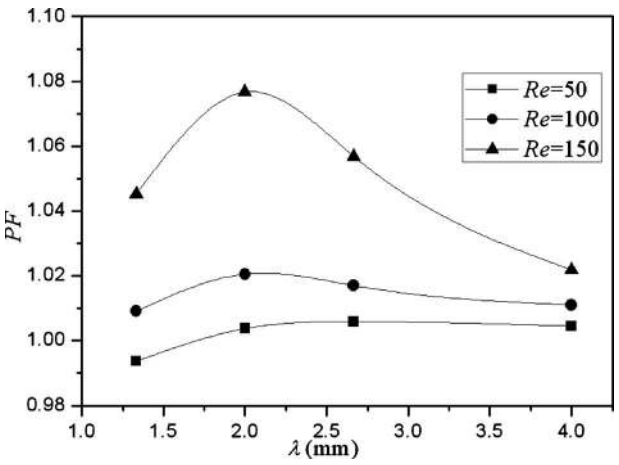

Fig. 13 Variation in *PF* with λ

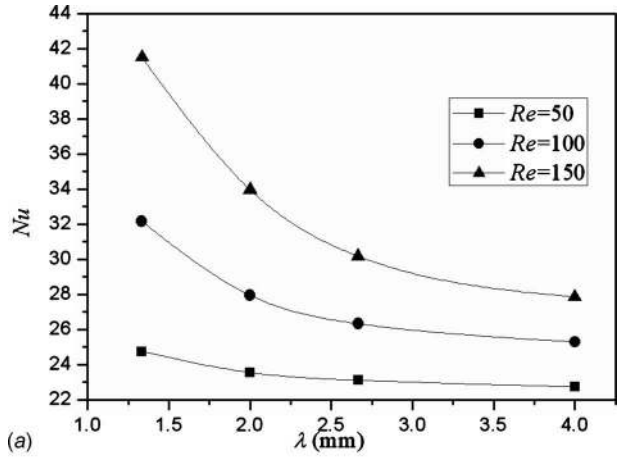

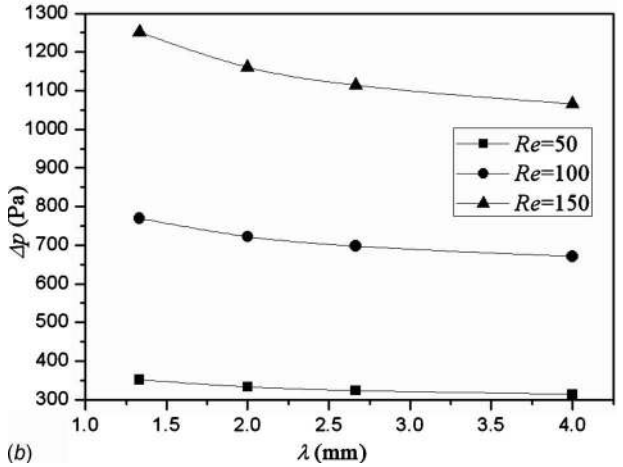

Fig. 14 Variation in (*a*) average Nusselt number and (*b*) pressure drop with wavelength

Nusselt number is plotted as a function of the channel length in Fig. 24. Enhancement can be observed for channel with high α. Due to the enhanced heat transfer for channels with high α, it was found that the maximum temperature also decreases as α and Re increase.

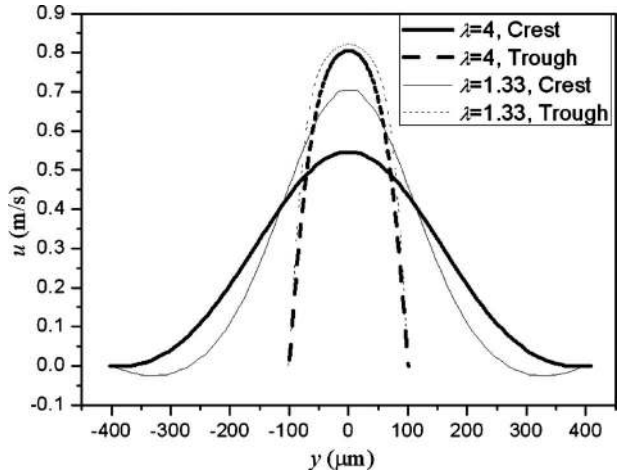

Fig. 15 Spatial velocity contours for different wavelengths

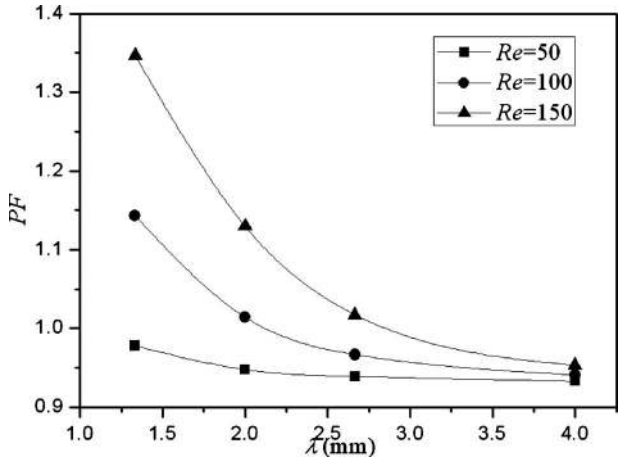

Fig. 16 Variation in *PF* with λ

4 Conclusions

Passive heat transfer enhancement in the form of wavy walls in microchannels for electronics cooling is pursued in the present paper. Rectangular cross section channels of hydraulic diameter 500 μm were considered and low Reynolds number ($50 \leq Re \leq 150$) liquid flow in laminar regime was studied using 3D CFD/heat transfer (HT) numerical simulations.

It was found that wavy surfaces can be potential candidates for performance improvement in low Re laminar flow regime with proper tuning and selection of the geometry and flow parameters without employing any extraneous mixing aids. In general, it was observed that $\Phi = \pi$ configuration performs better compared to $\Phi = 0$ configuration due to a lower rise in the pressure drop in the former case compared to the heat transfer improvement Under the considered conditions, for the better configuration ($\Phi = \pi$), the performance was found to improve with increase in Reynolds number (peak at Re=150) and the wave amplitude (peak at *A*

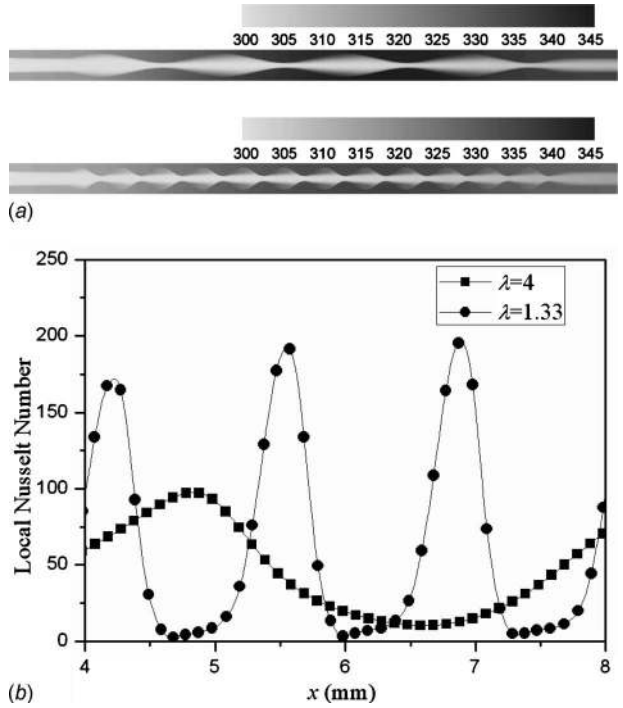

Fig. 17 (*a*) Temperature field for λ=4 (top) and λ=1.33 (bottom) and (*b*) local Nusselt number plot

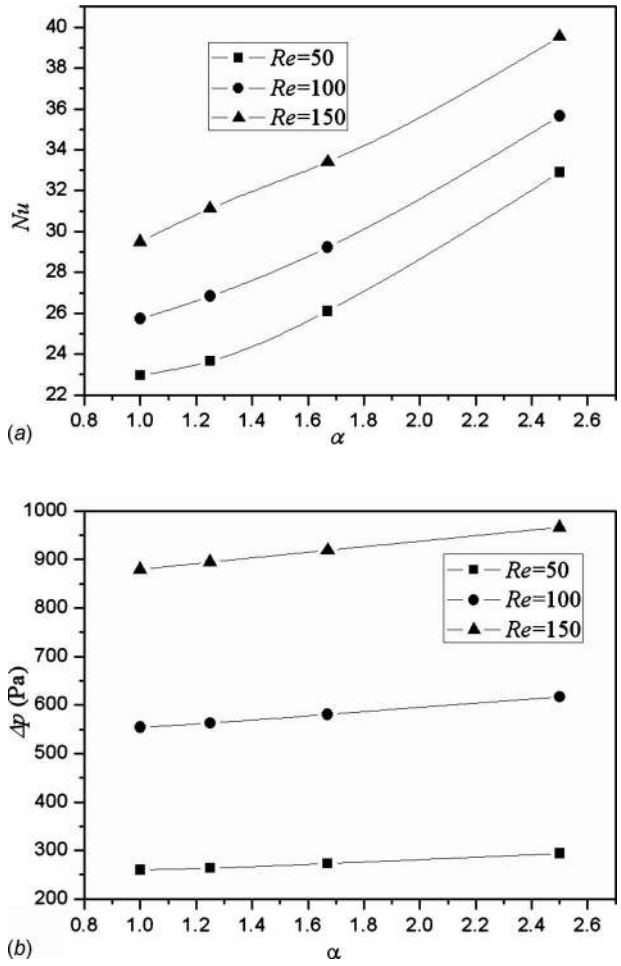

Fig. 18 Variation in (*a*) average Nusselt number and (*b*) pressure drop with aspect ratio

=200 μm) and vary with the wavelength (peak at $\lambda=2$ mm) and the aspect ratio (peak at $\alpha=1.3$). In general, higher wavelengths and more rectangular channels showed less potential for performance improvement. The better performance of large amplitude and small wavelength channels was ascribed to the thinning of boundary layer at the wave peaks as a result of the compounding effect of geometry and the flow velocity. Performance dependence on channel aspect ratio was found to be consistent with conventional observations in microchannel flows up to a certain aspect ratio but found to follow a reverse trend for high aspect ratios due to an increase in the pressure drop when Re is kept the same.

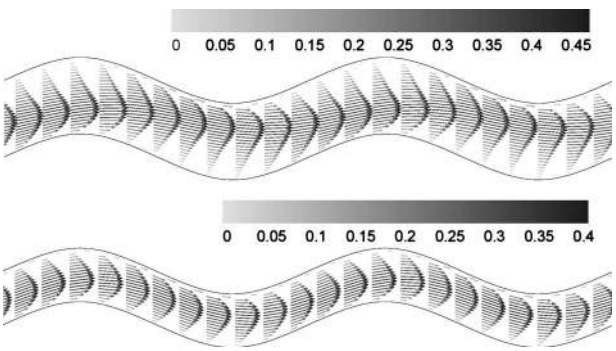

Fig. 19 Velocity vectors for $\alpha=1$ (top) and $\alpha=2.5$ (bottom)

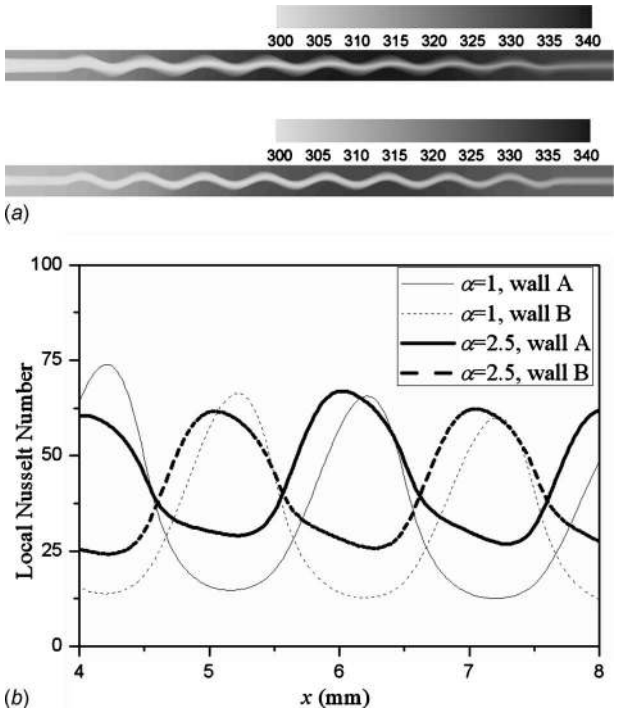

Fig. 20 (*a*) Temperature field for $\alpha=1$ (top) and $\alpha=2.5$ (bottom) and (*b*) local Nusselt number plot

In summary, the performance of wavy channels compares or exceeds the performance of a straight channel for $\mathrm{Re} \geq 50$ by up to 55% for the best case considered in this paper. The performance of wavy channels depends on the flow conditions, and with proper tailoring and optimization of the wavy features, it is anticipated that wavy microchannels can show enhanced performance over traditional microchannels, and can be an attractive choice for cooling of future microelectronics.

Acknowledgment

L.G. wishes to thank the China Scholarship Council and Georgia Tech for providing the financial support.

Nomenclature

A = wave amplitude, m
c_p = specific heat (at constant pressure) of the working fluid, J/kg·K

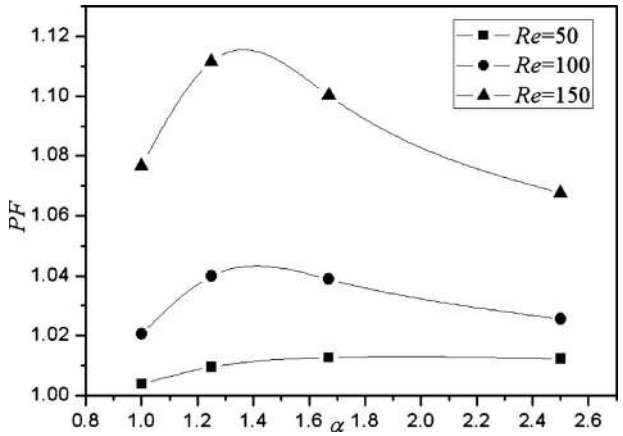

Fig. 21 Variation in *PF* with α

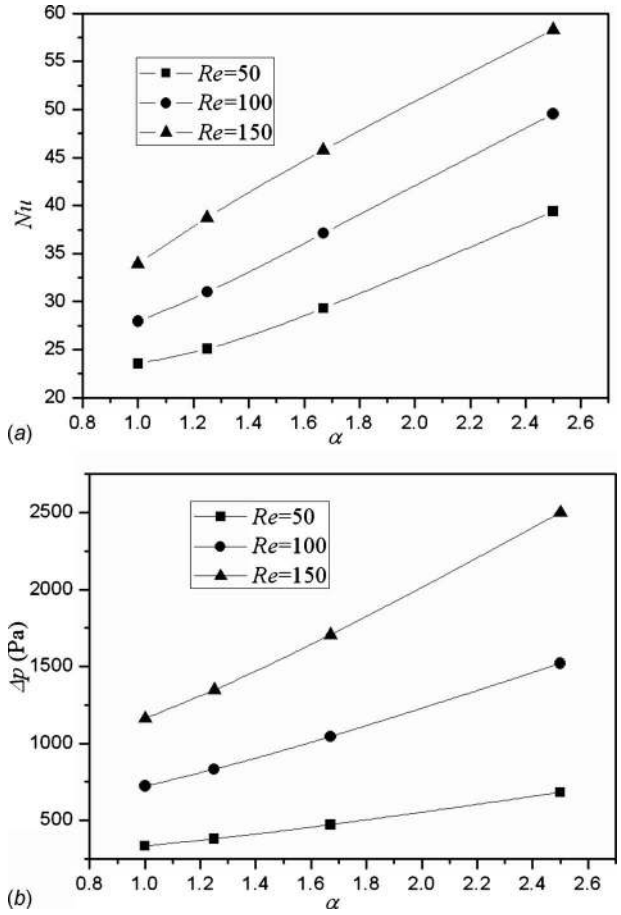

Fig. 22 Variation in (*a*) average Nusselt number and (*b*) pressure drop with aspect ratio

D = hydraulic diameter, m
H = channel height, m
k = thermal conductivity of the working fluid, W/m·K
L = channel length, m
Nu = Nusselt number averaged on the heated channel wall
p = static pressure, Pa
PF = performance factor
Re = Reynolds number

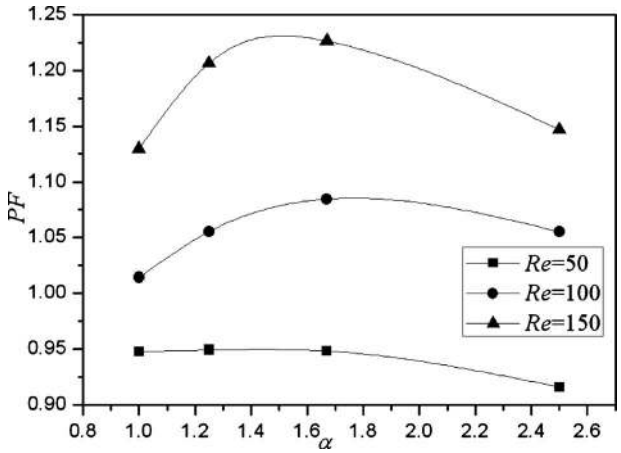

Fig. 23 Variation in *PF* with α

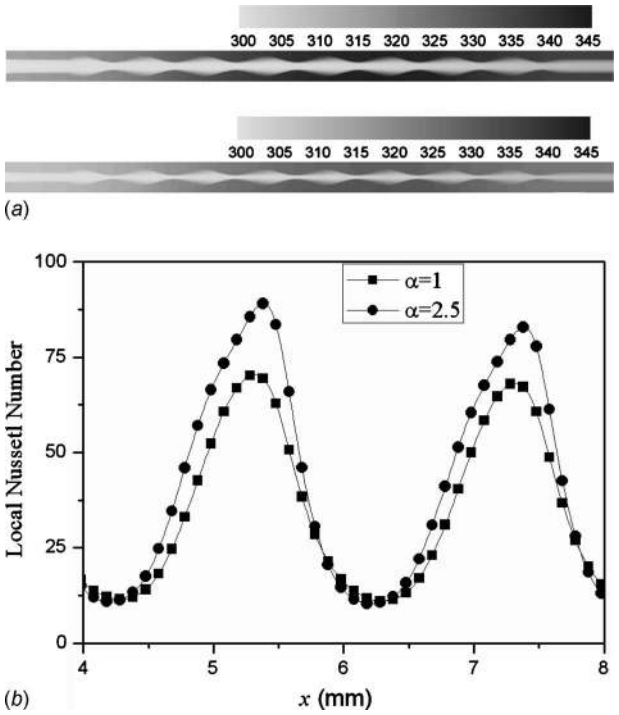

Fig. 24 (*a*) Temperature field for α=1 (top) and α=1.67 (bottom) and (*b*) local Nusselt number plot

W = channel width, m
x = Cartesian x-coordinate, m
y = Cartesian y-coordinate, m
z = Cartesian z-coordinate, m

Greek Symbols

Δ = difference in the value of a variable between inlet and outlet of a channel
Φ = phase angle
α = channel aspect ratio (=H/W)
ε = relative error in the fundamental variables in the numerical simulation
λ = wavelength or pitch of the wavy channel, m (also, represented as WL)
ρ = density of the working fluid, kg/m^3

Subscripts

w = wavy channel
s = straight channel

References

[1] www.itrs.net
[2] Xin, R. C., and Tao, W. Q., 1988, "Numerical Prediction of Laminar Flow and Heat Transfer in Wavy Channels of Uniform Cross-Sectional Area," Numer. Heat Transfer, **14**, pp. 465–481.
[3] Chen, C. K., and Cho, C. C., 2008, "A Combined Active/Passive Scheme for Enhancing the Mixing Efficiency of Microfluidic Devices," Chem. Eng. Sci., **63**, pp. 3081–3087.
[4] Henning, T., Brandner, J. J., and Schubert, K., 2005, "High-Speed Imaging of Flow in Microchannel Array Water Evaporators," Microfluid. Nanofluid., **1**, pp. 128–136.
[5] Kowalewski, T. A., Szumbarski, J., and Blonski, S., 2008, "Low-Reynolds-Number Instability of the Laminar Flow between Wavy Walls," *Proceedings of the Sixth International ASME Conference on Nanochannels, Microchannels and Minichannels*, Darmstadt, Germany, Jun. 23–25.
[6] Hsieh, S. S., and Huang, Y. C., 2008, "Passive Mixing in Micro-Channels With Geometric Variations Through μPIV and μLIF Measurements," J. Micromech. Microeng., **18**, p. 065017.
[7] Quddus, N. A., Bhattacharjee, S., and Moussa, W., 2005, "Electrokinetic Flow in a Wavy Channel," *Proceedings of the 2005 International Conference on MEMS, NANO and Smart Systems*, pp. 219–220, Alberta, Canada, Jul. 24–27.
[8] Xia, Z., Mei, R., Sheplak, M., and Fan, Z. H., 2009, "Electroosmotically

Driven Creeping Flows in a Wavy Microchannel," Microfluid. Nanofluid., **6**, pp. 37–52.
[9] Sui, Y., Teo, C. J., Lee, P. S., Chew, Y. T., and Shu, C., 2010, "Fluid Flow and Heat Transfer in Wavy Microchannels," Int. J. Heat Mass Transfer, **53**, pp. 2760–2772.
[10] Brunschwiler, T., Michel, B., Rothuizen, H., Kloter, U., Wunderle, B., Oppermann, H., and Reichl, H., 2008, "Forced Convective Interlayer Cooling in Vertically Integrated Packages," *2008 Proceedings of the ITHERM*, pp. 1114–1125.
[11] Sekar, D., King, C., Dang, B., Spencer, T., Thacker, H., Joseph, P., Bakir, M., and Meindl, J., 2008, "A 3D-IC Technology With Integrated Microchannel Cooling," *Proceedings of IEEE International Interconnect Technology Conference*, pp. 13–15.
[12] Coskun, A., Ayala, J., Atienzaz, D., and Rosingy, T., 2009, "Modeling and Dynamic Management of 3D Multicore Systems With Liquid Cooling," *Proceedings of the 17th Annual IFIP/IEEE International Conference on Very Large Scale Integration*, Brazil.
[13] Jang, H., Yoon, I., Kim, C., Shin, S., and Chung, S., 2009, "The Impact of Liquid Cooling on 3D Multi-Core Processors," *Proceedings of the 27th IEEE International Conference on Computer Design*, Lake Tahoe, CA, Oct. 4–7.
[14] Koo, J., Im, S., Jiang, L., and Goodson, K. E., 2005, "Integrated Microchannel Cooling for Three-Dimensional Electronic Circuit Architectures," ASME J. Heat Transfer, **127**(1), pp. 49–58.
[15] Fluent, Inc., 2003, Fluent 6 User Manual.
[16] Patankar, S. V., 1980, *Numerical Heat Transfer and Fluid Flow*, 1st ed., Taylor & Francis, London, UK.
[17] Gee, D. L., and Webb, R. L., 1980, "Forced Convection Heat Transfer in Helically Rib-Roughened Tubes," Int. J. Heat Mass Transfer, **23**, pp. 1127–1136.
[18] Berger, S. A., Talbot, L., and Yao, L.-S., 1983, "Flow in Curved Pipes," Annu. Rev. Fluid Mech., **15**, pp. 461–512.